Photopolymerization-Induced Crystallization in Relation to Solid−Liquid Phase Diagram of Poly(ethylene oxide)/Diacrylate Monomer Blends

Soo Jeoung Park and Thein Kyu*

Department of Polymer Engineering, University of Akron, Akron, Ohio 44325

Received September 23, 2008; Revised Manuscript Received November 18, 2008

ABSTRACT: Phase diagrams of blends of poly(ethylene oxide) (PEO)/diacrylate (DA) monomer have been established by means of differential scanning calorimetry and optical microscopy. A phase field theory based on the combination of the phase field free energy of crystal solidification and the Flory−Huggins theory for liquid−liquid phase separation has been developed that is capable of predicting various coexistence regions of the binary crystalline PEO/DA blends, viz., isotropic (I), the coexistence of crystal + liquid (Cr_1 + I), crystal + crystal (Cr_1 + Cr_2), and the single phase crystal (Cr) regions. These aforementioned coexistence regions have been further verified experimentally by probing the spatiotemporal emergence of crystalline structure and phase morphology. Guided by these established phase diagrams of the PEO/diacrylate blends, photopolymerization-induced crystallization experiments have been carried out at the isotropic temperatures slightly above the depressed melting points of PEO crystals. Of particular interest is the development of spherulites in the continuum of isotropic in the crystal + liquid coexistence region, whereas viscous fingering (or fractal growth) occurs during photopolymerization at a higher temperature, showing phase-separated domains within these advancing viscous fingering structures.

Introduction

In recent years, miscibility phase diagrams of crystalline polymer blends, especially binary crystalline/crystalline mixtures, have received considerable attention due to a variety of coexistence regions and phase morphologies displayed by these systems.[1−7] To elucidate these morphology phase diagrams, a phase field theory of crystal solidification in binary crystalline polymer blends has been introduced by Matkar and Kyu[8,9] by combining the Flory−Huggins free energy for amorphous−amorphous isotropic mixing[10] and the Landau free energy of crystal solidification.[11−13] Of particular importance is that their model takes into consideration all possible interactions including amorphous−amorphous, crystalline−amorphous, amorphous−crystalline, liquid−liquid, and crystalline−crystalline interactions.[8,9] Subsequently, it was demonstrated that the self-consistent solution of the phase diagram calculation reveals various coexistence regions consisting of liquid + liquid, liquid + solid, and solid + solid coexistence regions bound by the liquidus and solidus lines.

In this article, the phase diagram of poly(ethylene oxide) (PEO)/diacrylate (DA) blends has been determined by means of differential scanning calorimetry (DSC) and time-resolved optical microscopy (OM). This binary crystalline−crystalline polymer blend is of particular interest by virtue of photopolymerizability of DA that permits fabrication of photonic crystals via photolithography and also crystalline nature of both constituents. While the phenomenon of polymerization-induced phase separation has been well investigated experimentally and theoretically,[14−18] the phenomenon of polymerization-induced crystallization is relatively new.[19] The concept of polymerization-induced crystallization is similar to that of reaction-induced liquid−liquid phase separation in binary polymer blends, except that polymer crystallization can take place when the originally depressed melting transition curve moves upward to an elevated temperature and eventually surpasses the reaction temperature during photoinitiated free radical polymerization.[19] The spatiotemporal development of diverse hierarchical morphologies of the PEO/DA system is analyzed in relation to the solid−liquid phase diagram following thermal quenching into various coexistence regions as well as during photopolymerization of DA in the isotropic melt of the blends.

Theoretical Scheme

To establish the crystal−melt coexistence regions pertaining to the solid−liquid phase transitions, the Flory−Huggins (FH) theory[10] of liquid−liquid demixing is combined with the crystal solid−amorphous liquid phase separation by taking into consideration the crystalline−amorphous melt and crystalline−crystalline interactions[8,9] in addition to the conventional amorphous−amorphous interaction. The total free energy density of mixing of such crystalline−amorphous polymer blend consists of the free energy density pertaining to crystal order parameter of the crystalline constituent weighted by its volume fraction (ϕ) and the FH free energy of liquid−liquid demixing, viz.[9]

$$f(\psi_1,\phi) = \phi f(\psi_1) + (1-\phi) f(\psi_2) + \frac{\phi}{r_1}\ln(\phi) + \frac{1-\phi}{r_2}\ln(1-\phi) + \{\chi_{aa} + \chi_{ca}\psi_1^{\,2} - \chi_{cc}\psi_1\psi_2 + \chi_{ac}\psi_2^{\,2}\}\phi(1-\phi) \quad (1)$$

where χ_{aa} is the FH interaction parameter representing the amorphous−amorphous interaction of the constituent chains in the isotropic melt, χ_{ca} represents the crystalline−amorphous interaction parameter of crystalline phase of constituent 1 and amorphous constituent 2, and χ_{ac} is that of amorphous phase of constituent 1 and the crystalline phase of constituent 2. The crystal phase order parameter (ψ_1) can be given as the ratio of the lamellar thickness (l_1) of the first constituent to the lamellar thickness of a perfect crystal (l_1^0), i.e., $\psi_1 = l_1/l_1^0$, and thus it represents the linear crystallinity (i.e., one-dimensional crystallinity) of the crystallizing component.[8,9] r_1 and r_2 represent the number of the statistical segments or the lattice sites occupied

* To whom correspondence should be addressed.

10.1021/ma802161c CCC: $40.75
Published on Web 01/22/2009

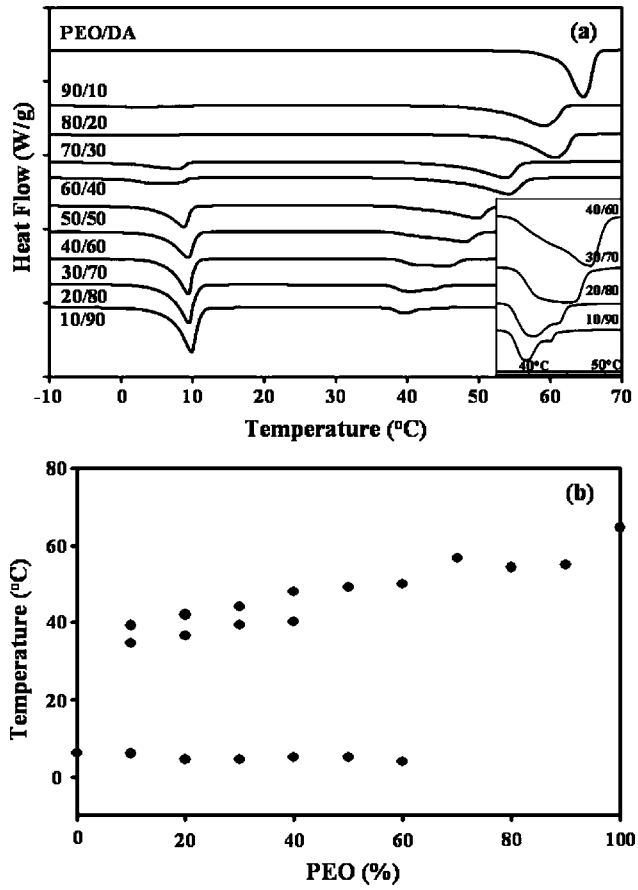

Figure 1. (a) DSC thermograms of PEO/DA blends obtained at a heating rate of 2 °C/min, showing a systematic movement of the melting peaks of PEO and of DA as a function of blend ratio. The inset represents the enlarged dual melting peaks of PEO in the blends. (b) Plots of melting temperatures of PEO/DA blends versus PEO volume fraction obtained at 2 °C/min.

by the crystalline polymer and of the monomer constituents, respectively. Note that the order of the subscripts denotes the constituent 1 (crystalline polymer) and constituent 2 (crystalline monomer).

To clarify the physical essence of the enthalpic contribution, eq 1 may be rewritten as

$$f(\psi_1,\phi) = \phi f(\psi_1) + (1-\phi)f(\psi_2) + \frac{\phi}{r_1}\ln(\phi) + \frac{1-\phi}{r_2}\ln(1-\phi) + \chi_{aa}\phi(1-\phi) + \chi_{ca}[\phi\psi_1][(1-\phi)\psi_1] - \chi_{cc}[\phi\psi_1][(1-\phi)\psi_2] + \chi_{ac}[(1-\phi)\psi_2][\phi\psi_2] \quad (2)$$

where the product of ϕ and ψ_1 in the last term of eq 2 corresponds to the bulk crystallinity of the constituent 1 in the blend, whereas the product of $(1-\phi)$ and ψ_1 implies the amount of amorphous materials interacting with the crystalline phase, and hence the last term, $\chi_{ca}\phi\psi_1(1-\phi)\psi_1$, signifies the repulsive crystal−amorphous interaction. The same argument applies to the second crystalline constituent. In the case of cocrystals, the terms $[\phi\psi_1]$ and $[(1-\phi)\psi_2]$ represent the crystallinity of each crystalline constituent, and χ_{cc} representing the strength of crystal−crystal interaction within the cocrystals may be expressed according to the geometric means, i.e., $\chi_{cc} = c_\omega(\chi_{ca}\chi_{ac})^{1/2}$, where $c_\omega = 1$ signifies the ideal case and $c_\omega = 0$ indicates the complete immiscibility between the individual crystalline phases, forming separate crystals; viz., χ_{ca} and χ_{ac} may be treated as independent.[9] Since the cocrystals are rare to come by for most crystalline

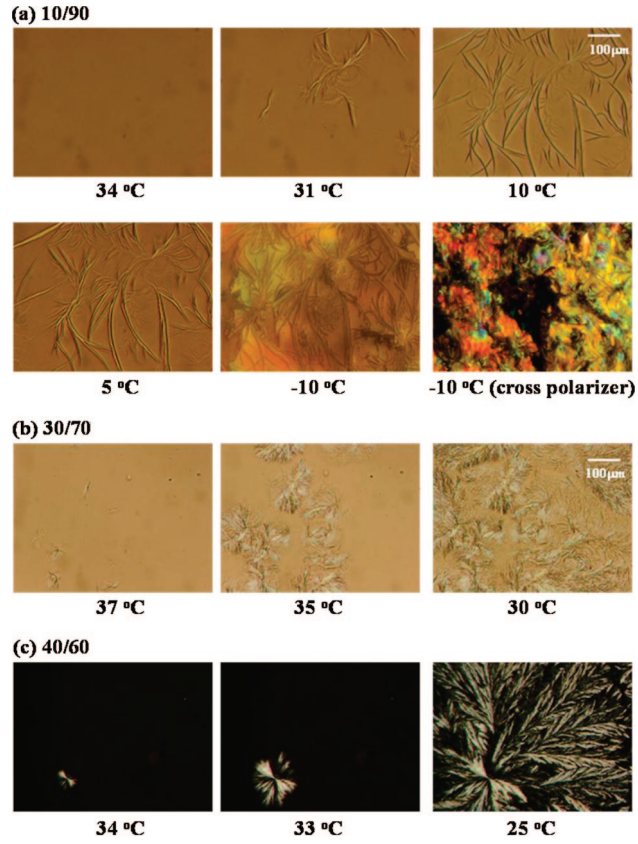

Figure 2. Optical micrographs of PEO/DA (a) 10/90, (b) 30/70, and (c) 40/60 during cooling from isotropic melt (100 °C) to various temperatures at rate of 1 °C/min.

polymer blends, the crystal−crystal interaction term may simply be dropped from eq 1 like in the present case.

The aforementioned crystal order parameter (ψ) may be described in the context of phase field based on the Landau free energy,[13] viz.

$$f(\psi_i) = W_i\left[\frac{\zeta_i(T)\zeta_{i,0}(T_{m,i})}{2}\psi_i^2 - \frac{\zeta_i(T)+\zeta_{i,0}(T_{m,i})}{3}\psi_i^3 + \frac{1}{4}\psi_i^4\right] \quad (3)$$

where the parameter ζ_i represents the unstable hump for the crystal nucleation and W_i is the coefficient that represents the penalty to overcome the energy barrier for the nucleation process. $\zeta_{i,0}$ represents the crystal order parameter at the solidification potential of crystallization. These coefficients of the Landau free energy expansion are treated as temperature dependent so that the free energy has the form of an asymmetric double well at a given crystallization temperature or supercooling, but it reverts to the symmetric double well at equilibrium. It should be cautioned that the coefficient of the cubic power term must be nonzero in order to apply the Landau potential to the first-order phase transition;[11−13] otherwise, eq 3 is applicable only to a second-order phase transition.

Regarding determination of the crystal−liquid (melt) phase transition of the constituents, the free energy was first minimized with respect to the individual crystal order parameters for each temperature, i.e.

$$\frac{\partial f(\psi_i)}{\partial \psi_i} = W_i[\psi_i^2 - (\zeta_i + \zeta_{i,0})\psi_i + \zeta_i\zeta_{i,0}] + 2\chi_{ca,i}(1-\phi_i) = 0 \quad (4)$$

The free energy penalty representing the solidification hump (barrier), W, is related to the heat of fusion, ΔH_u, as follows:[27]

$$W_i = \frac{6\Delta H_{u,i}}{RT}\left(1 - \frac{T}{T^0_{m,i}}\right)\left(\frac{1}{2} - \zeta_i\right)^{-1} \quad (5)$$

where R is the gas constant and the two bracket terms signify correction for the supercooling effects. At equilibrium, W_i is reduced to $W_i = 6\Delta H_{u,i}/RT$, but eq 5 must be used for the nonequilibrium and nonlinear dynamical processes. To determine the coexistent points, the equilibrium value of the crystal order parameter, ψ_ι thus obtained for each blend composition (ϕ_ι) was subsequently substituted in the free energy expression, and then the pseudo-chemical potentials at each phase were balanced as follows:

$$\frac{\partial f_i}{\partial \phi_\iota}^{\alpha} = \frac{\partial f_i}{\partial \phi_\iota}^{\beta} \quad (6)$$

In the determination of the coexistence curves, a common tangent algorithm was employed; the detailed description of the aforementioned approach may be found elsewhere.[8,9]

Experiment

Materials and Methods. Poly(ethylene oxide) (PEO), purchased from Scientific Polymer Products, Inc., has a reported weight-average molecular weight (M_w) of 66 000 g/mol with a polydispersity of 1.94. 1,6-Hexanediol diacrylate (DA) having M_w of 226 g/mol with a density of 1.01 g/mL was purchased from Aldrich Chemical Co. Various concentrations of PEO were dissolved in diacrylate monomer by mixing at room temperature in hot water bath controlled at ≈70 °C on a hot plate using a magnetic stirrer bar. These PEO/DA blend specimens were solvent cast at ambient temperature for thermal and optical investigations.

Nonisothermal crystallization experiments were carried out using differential scanning calorimetry (Model Q-1000, TA Instruments). Samples weighing 7−10 mg were encapsulated in aluminum hermetic DSC pans, and nitrogen gas was purged to the unit to maintain an inert atmosphere. Indium standard was used for temperature and heat flow calibration. DSC scans were carried out for whole PEO/DA mixtures at various heating rates (e.g., 2, 5, and 10 °C/min); only the thermograms from the second heating scan were considered in the analysis. The development of crystalline structure and phase-separated domain morphology was examined using OM (Olympus-BX60) equipped with a hot stage (TMS 93, Linkam).

Regarding photopolymerization, Rose Bengal photoinitiator[20] (1 wt % of reactive monomer) was utilized with the aid of *N*-phenylglycine (co-initiator), *N*-vinylpyrrolidone (solubilizing agent), and octanoic acid (surfactant).[21] The Rose Bengal ester possesses two broad absorptions in the regions of 350−440 and 450−560 nm having a high triplet quantum yield of 0.76.[20] However, the filtered green light with a wavelength of 532 nm was utilized in the microscopic studies of polymerization-induced phase transitions of the present PEO/DA system.

Results and Discussion

Phase Transition and Morphology Phase Diagram. Figure1a exhibits the DSC thermograms of the PEO/DA blends obtained for the entire composition range with 10 wt % increments at 2 °C/min. The melting transition temperature (T_m) of the neat PEO was 65 °C. With increasing DA concentration, the endothermic peak of PEO crystal systematically shifts to lower temperatures, but the endothermic peak widens slightly. This observed lowering trend of the melting point of PEO with DA content is consistent with those reported for other miscible or partially miscible blends, except that there appear dual melting peaks of PEO in the thermograms, especially at low PEO concentrations. Such dual peaks can be seen more clearly in the enlarged scale depicted in the inset. On the other hand, the melting peak of neat DA was ≈10 °C, but it shows little or no movement upon blending with PEO. In view of the nonequilibrium nature of these melting peaks, additional DSC runs were performed at 5 and 10 °C/min; these dual peaks at low PEO concentrations are found to be reproducible.

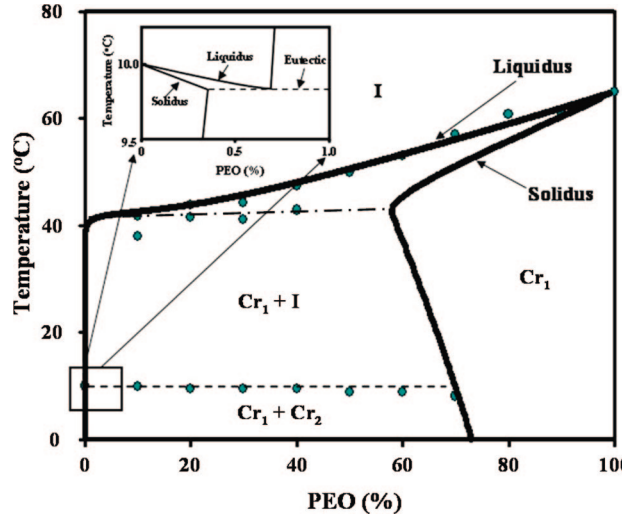

Figure 3. Comparison between self-consistent solution (solid lines) and experimental melting temperatures of PEO/DA blends, showing the liquidus and solidus lines merging with the coexistence lines of the UCST. The two horizontal lines show the monotectic and eutectic lines in the descending order of temperature. The heat of fusions of PEO and DA were $\Delta H_{1,u} = 8.36$ kJ/mol and $\Delta H_{2,u} = 2.05$ kJ/mol, respectively. Other parameters used were $r_1 = 110$, $r_2 = 1$, $\chi_{ac} = 0.01$, $\chi_{ca} = 0.27$, $\chi_{aa} = 0.61$ at 40 °C and $A = -0.9$ and $\chi_{cc} = 0.0001$ at $T_{crit} = 42$ °C. The inset shows the solidus and liquidus lines near the DA crystal region.

Similar melting point depression phenomena have also been reported in other binary crystalline polymer blends.[22−27] Regarding miscible blends, the melting point of the crystalline component is usually lowered relative to the pure polymer as a result of thermodynamically favorable interactions between the crystal and the surrounding amorphous constituent. Thus, the melting point depression has been used extensively to evaluate the miscibility of polymer blends. In addition to the thermodynamic effect on the melting point depression, morphological variables such as lamellar thickness and crystal perfection can profoundly affect the melting point.

Figure 1b shows the composition dependence of T_m of PEO/DA blend. The pseudo-equilibrium melting points (T^0_m) were obtained by extrapolating the T_m at various heating rates to zero heating rate; the superscript indicates the extrapolated zero heating rate. A similar attempt has been made to estimate the pseudo-equilibrium crystallization temperature, T_c; however, the determination of the equilibrium phase transition temperature is usually ambiguous due to the nonequilibrium nature of polymer crystallization, which strongly depends on supercooling, cooling rate, and also the crystalline morphology such as crystal perfection and lamellar thickness, among others. Hence, only the pseudo-equilibrium crystal-melting temperatures of PEO and DA as obtained from the DSC studies are shown in the phase diagram. The dual melting peaks of a neat crystalline polymer have been customarily interpreted as due to the melting point depression or the phase transformation of different crystal modifications. In small molecule crystal mixtures, such dual melting peaks have been attributed to the liquidus and solidus phases,[28] which have been shown to be adequate for describing the eutectic crystals of various crystalline polymer blends.[23−27]

Morphology development during crystallization was determined as a function of composition using optical microscopy (OM). The progression of crystalline texture from a needlelike lamellar crystal can be discerned in the 10/90 PEO/DA during

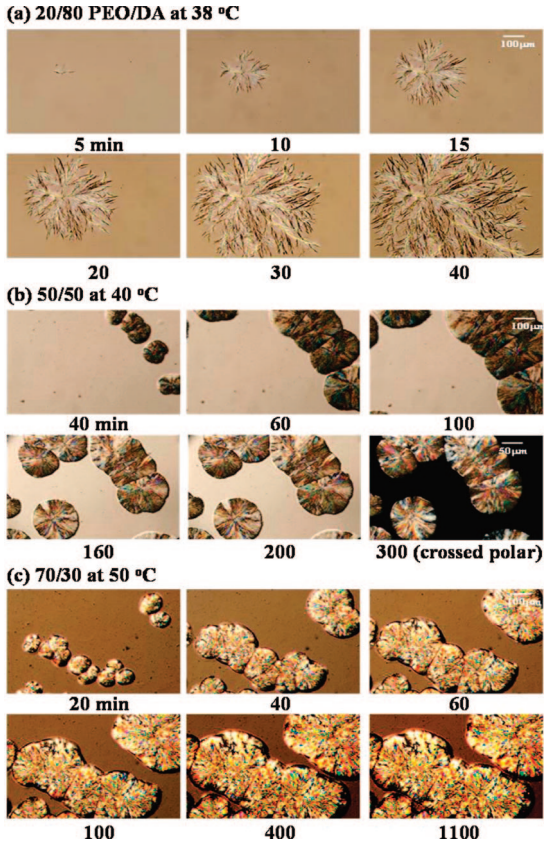

Figure 4. Time evolution of the crystalline structure of PEO in the blend of the PEO/DA at an isothermal crystallization temperature of (a) the 20/90 PEO/DA blend at 38 °C showing the evolution of needlelike structure, (b) the 50/50 PEO/DA blend at 40 °C showing the evolution of spherulite structure, and (c) the 70/30 blend exhibiting the evolution of spherulite structure at 50 °C verifying the regions of PEO crystal and DA-rich liquid phase, representing the crystal + liquid coexistence gap bound by the liquidus and solidus lines.

the course of cooling (Figure 2a). These lamellar aggregates continue to grow through splitting and branching upon cooling to 10 and 5 °C. When the temperature reaches around −10 °C, it suddenly shows birefringent appearance indicative of the development of the DA crystal (Figure 2a). The emergence of hierarchical morphology of PEO crystals can be witnessed in the 30/70 PEO/DA blend (Figure 2b), showing the development of sheaflike structure or incomplete spherulite at 30 °C. In Figure 2c, the 40/60 blend shows the temporal growth of PEO spherulite, having an open spherulitic morphology. As expected, the crystalline morphology of the binary blend is strongly influenced by both composition and temperature of crystallization. Although these emerged crystalline morphologies roughly correspond to various coexistence regions of the phase diagram of PEO/DA, the slow cooling process is by no means equilibrium.

To substantiate these coexistence regions, the melting temperatures are plotted against composition in Figure 3 in comparison with the solid−liquid phase transition. The theoretical solidus and liquidus lines were obtained by self-consistently solving the combined phase field free energy and the Flory−Huggins (FH) free energy of liquid−liquid phase separation, i.e., eq 2. The heat of fusions of neat PEO and DA were $\Delta H_{1,u} = 8.36$ kJ/mol and $\Delta H_{2,u} = 2.05$ kJ/mol, respectively. The interaction parameters of crystal−amorphous and amorphous−crystal were taken as $\chi_{ca} = 0.27$ and $\chi_{ac} = 0.01$, respectively. The amorphous−amorphous interaction parameter was set at $\chi_{aa} = 0.61$ along with other parameters, viz., $A = -0.9$, $r_1 = 110$ for PEO and $r_2 = 1$ for DA at $T_{crit} = 42$ °C.

As depicted in Figure 3, the self-consistent solution reveals a solid−liquid coexistence gap bound by the solidus and liquidus lines intersecting with the upper critical solution temperature (UCST). The close resemblance of the predicted liquidus line and the monotectic line (i.e., the horizontal dash-dot line) to the experimental melting transition points is promising. Moreover, the present theoretical prediction is in good agreement with the experimental observations on various crystalline polymer blends reported by Smith and Manley[23] as well as by Guenet et al.[24−27] The solidus points were very rare to come by experimentally,[23−28] and thus it is not unusual to draw these solidus lines by hand.[24−27] The present self-consistent approach permits the determination of both liquidus and solidus lines simultaneously, and thus it is consistent with other binary systems such as metal alloys or liquid crystalline mixtures. More importantly, the present theory can remedy one deficiency of the original Flory diluent theory that predicts only a single liquidus line. The predicted coexistence regions include isotropic (I), the coexistence of crystal + liquid (Cr_1 + I), and crystal + crystal (Cr_1 + Cr_2) regions. The two horizontal lines represent the monotectic line (upper) and the eutectic line (lower). The isotropic liquid line of the Cr_1 + I gap is virtually coincided with the pure DA axis, and thus it may be regarded as L_2. Although the single phase crystal of PEO (Cr_1) is clearly discernible, the Cr_2 region (corresponding to the DA crystal phase) can be seen only in the enlarged version in the inset.

To identify these theoretically calculated regions, several temperature quenches were performed from the isotropic melt (i.e., 80 °C) to various temperatures at different compositions within the crystal + isotropic liquid region bound by the liquidus line and solidus line. Figure 4a displays the time sequence of spherulitic crystalline morphologies in the blend of PEO/DA 20/80 following a temperature quench from the isotropic melt (80 °C) to 38 °C. Thin lamellae initially develop and radiate from a common center via branching within 5 min. Subsequently, the lamellae further aggregate while branching continues (please see the picture at 10 min). With elapsed time, the initial lamellae gradually evolve finally to an open spherulitic structure through branching. More importantly, these hierarchical spherulites are surrounded by the isotropic melt, which is the signature of the Cr_1 + I region.

In the case of 50/50 PEO/DA blend, it shows the growth of the dense spherulite structures in the continuum of the isotropic DA-rich melt as demonstrated in Figure 4b. Similarly, the 70/30 PEO/DA mixture reveals the progression of dense spherulitic morphology (Figure 4c). Of particular interest is that the emerged spherulitic morphology shows little or no change from 400 to 1100 min, suggesting that the emerged two-phase structure probably reaches asymptotic equilibrium, which in turn confirms the crystal + liquid coexistence region.

Deeper thermal quenches were also performed into the crystal + liquid and crystal + crystal coexistences regions. Figure 5a−g exhibits the emerged morphologies in relation to the phase diagram of the PEO/DA blends. Upon quenching the 20/80 PEO/DA blend to 38 and 35 °C, the Cr_1 + I coexistence phases can be identified in the optical micrographs obtained (a) without and (b) with the crossed polarizers; the dark appearance under the crossed polarizers indicates the isotropic phase. The same conclusion can be reached for the 50/50 and 70/30 blends (see Figure 5c−f). When thermal quenching of the 70/30 blend was performed slightly below the solidus line to 45 °C, the whole microscopic view was volume-filled with solvated PEO spherulites, suggestive of the Cr_1 region. It seems that DA acts like a good solvent, which may be intimately mixed with the PEO spherulites. These morphology studies along with the DSC melting points confirmed the theoretically calculated various coexistence regions.

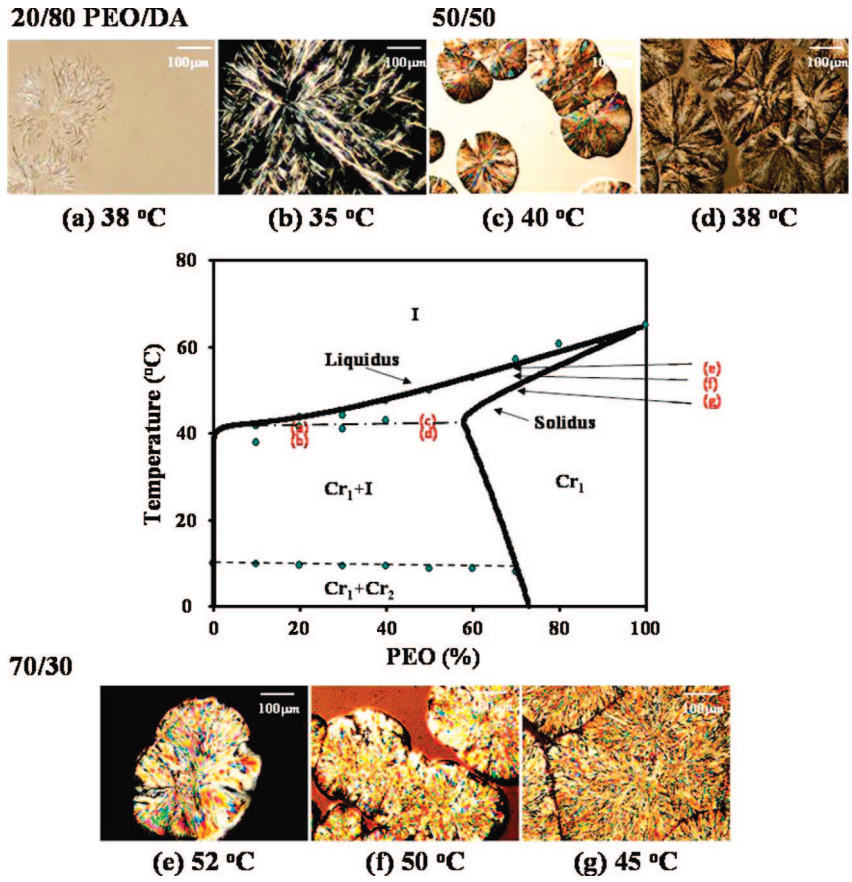

Figure 5. Emerged final crystalline morphologies of PEO/DA blends following the thermal quenching to various indicated temperatures showing (a−f) the coexistence of spherulitic crystals in the continuum of isotropic melt. The impinged spherulites in (g) represent the single phase PEO crystal region, as the quenching was performed just below the solidus line.

The dashed line in Figure 6 represents the eutectic line demarcating temperatures between $Cr_1 + I$ and $Cr_1 + Cr_2$. Upon quenching to 25 °C depending on PEO composition and the lower line distinguished the phase of Cr_1 from PEO and Cr_2 from DA crystals in accordance with DA crystal when the system quenched to −10 °C from the isotropic melt state. It should be noted that in the T quench of 70/30 to 38 °C the system passes from the isotropic state (I) to the crystal state ($Cr_1 + Cr_2$) through the crystal + isotropic liquid gap ($Cr_1 +$ I). As may be expected for the $Cr_1 + I$ region, the 10/90 and 20/80 blends show the aggregates of needle structures in the continuum of isotropic melt at 25 °C (Figure 6a,b). At 70/30, the fully developed spherulite PEO crystal can be seen as expected for the Cr_1 region. When these blends were quenched to around −10 °C, a different type of crystal develops, which may be attributed to that of DA, in conformity with the formation of separate crystals ($Cr_1 + Cr_2$) (Figure 6d−g). On the basis of these thermal quenched experiments, the emerged morphologies were found to accord well with the calculated coexistence regions pertaining to the solid−liquid phase diagram of the PEO/DA blends.

Morphology Development during Photopolymerization-Induced Crystallization. The photopolymerization-induced crystallization is governed by the instability induced by the increase in molecular weight and subsequent cross-linking reaction of the constituent reactive monomers. During photopolymerization, the depressed melting curve shifts upward to elevated temperatures and eventually surpasses the reaction temperature, which in turn thrusts the system into the unstable gap, thereby triggering the photopolymerization induced crystallization. Consequently, the value of r_2 changes from unity (i.e., for diacrylate) to r_p representing the number of statistical segment of the emerged polyacrylate, under the constraint that $\phi_2 = \phi_m + \phi_p$. Then the Flory−Huggins free energy of mixing of a crystalline polymer blend in the melt state may be expressed in terms of a ternary system, consisting of monomer, emerging polymer, and the crystalline constituent in the isotropic melt state in what follows:[19]

$$f_{mixing} = f(\phi) = \frac{\phi_1 \ln(\phi_1)}{r_1} + \phi_m \ln(\phi_m) + \frac{\phi_p \ln(\phi_p)}{r_p} + \chi_{aa}\phi_1(1 - \phi_1) \quad (7)$$

Assuming the equilibrium is reached at each conversion step, the total free energy of the polymerizing system may be expressed for each conversion as

$$f(\psi, \phi) = \frac{\phi_1 \ln(\phi_1)}{r_1} + \phi_m \ln(\phi_m) + \frac{\phi_p \ln(\phi_p)}{r_p} + \chi_{aa}\phi_1(1 - \phi_1) + W\phi_1\left(\frac{\zeta\zeta_0}{2}\psi^2 - \frac{\zeta + \zeta_0}{3}\psi^3 + \frac{1}{4}\psi^4\right) + \chi_{ca}\phi_1\phi_m\psi^2 \quad (8)$$

During the course of polymerization, the conversion (α) from monomer to emerging polymer can be expressed as follows:[18,19]

$$\alpha = \frac{\phi_2 - \phi_m}{\phi_2}, \quad \phi_p = \alpha\phi_2, \quad \text{or} \quad \phi_m = (1 - \alpha)\phi_2 \quad (9)$$

The rate of conversion of the monomer into polymer is described by the first-order reaction, and it is given as

$$\frac{d\alpha}{dt} = k(1 - \alpha) \quad (10)$$

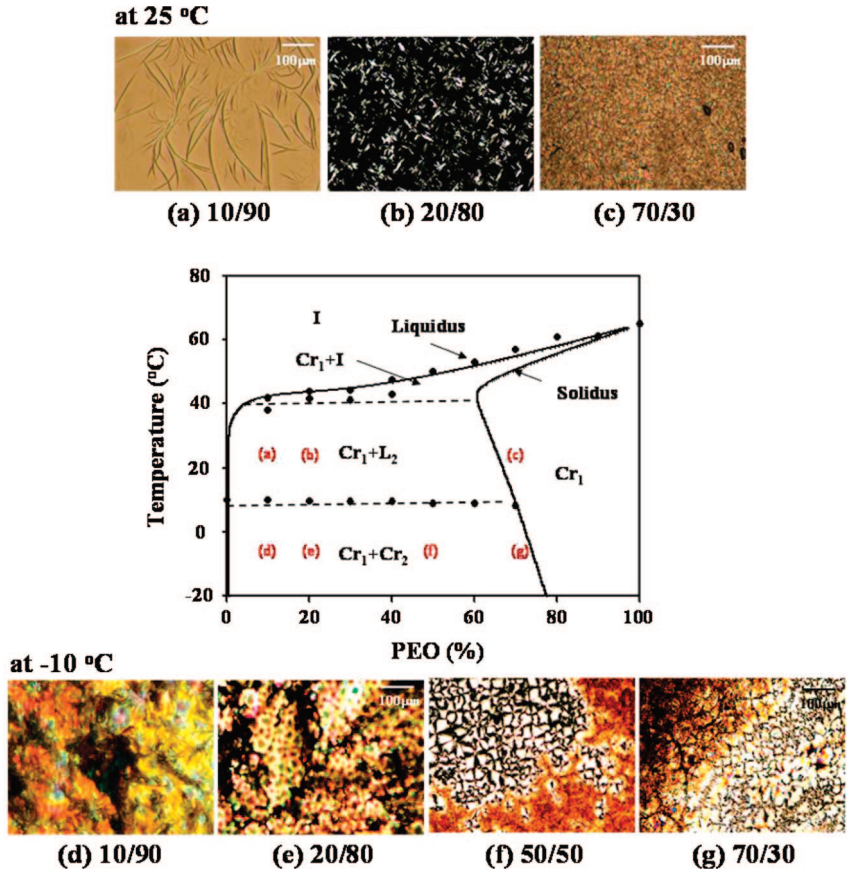

Figure 6. Emerged morphologies at various composition compositions after quenching to the indicated isothermal crystallization temperatures: (a) 10/90, (b) 20/80, and (c) 70/30, confirming the (Cr_1 + I) regions (upper row) and the single phase crystal at 70/30 and (d) 10/90, (e) 20/80, (f) 50/50, and (g) 70/30 verifying the coexistence of (Cr_1 + Cr_2) regions (bottom row).

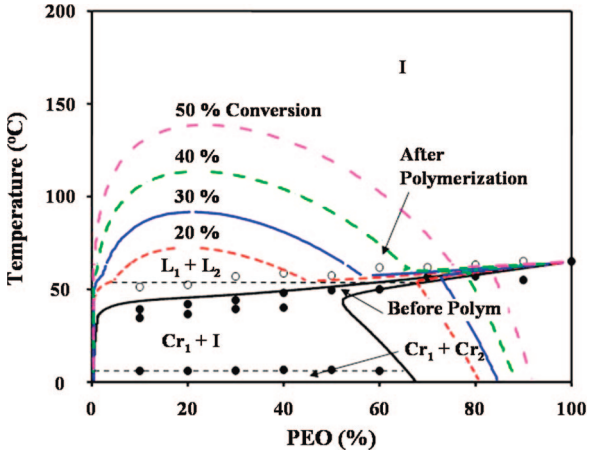

Figure 7. Starting phase diagram of the PEO/DA blend containing the photoinitiator diluent before the photopolymerization in conjunction with the snapshot phase diagrams evolving with the progression of the reaction (or conversions).

In actual photopolymerization, the lumped rate constant k is expressed in terms of the propagation and termination rate constants, i.e., $k = k_p/k_t^n$, where n is the reaction exponent and is 0.5 if one assumes the bimolecular termination reaction between macroradicals. The conversion rate is proportional to the one-half power of the intensity of irradiation, i.e., $I_a^{0.5}$, which may be valid in the initial stage of the reaction, but at the steady state where termination via trapping is competing with termination by combination, k changes with intensity with a power of unity, i.e., $I_a^{n=1}$. However, in practice, the combined monomolecular and bimolecular termination mechanisms may be a likely scenario for the termination process with the n value varying between 1/2 and 1.[29]

Figure 7 shows a self-consistently calculated phase diagram of the starting binary crystalline PEO/DA and the calculated snapshot phase diagrams during the course of photopolymerization. The calculated liquidus line was found to accord well with the depressed melting temperatures of the PEO/DA blends containing the photoinitiator syrup. With the progression of the reaction, the molecular weight of polyacrylate increases, which in turn acts as a driving force for the instability of the system. This reduction in the blend miscibility in turn pushes the depressed melting points to spring back toward their original values.

Now, let us consider an experiment where the reacting blend was set in the isotropic melt state slightly above the depressed melting transition of the PEO. With the progression of the reaction, both the UCST and the melting transition temperature increase beyond the reaction temperature. The supercooling created by the changing coexistence lines then triggers phase separation as well as crystallization, which will be hereafter called photopolymerization-induced phase separation and photopolymerization-induced crystallization, respectively. One can anticipate that the final morphology is determined by the competition between the relative rates of the above two processes in a manner dependent on the trajectory traversed by the system across the coexistence regions of the phase diagram.

Since the photoreaction rate depends on the intensity of illumination, one can anticipate discerning the directional growth of the microstructure from the nonuniform illumination, e.g., the intensity gradient.[19] Various blend samples were illuminated using a filtered green light at various temperatures, typically about 5 °C above their respective melting temperatures under

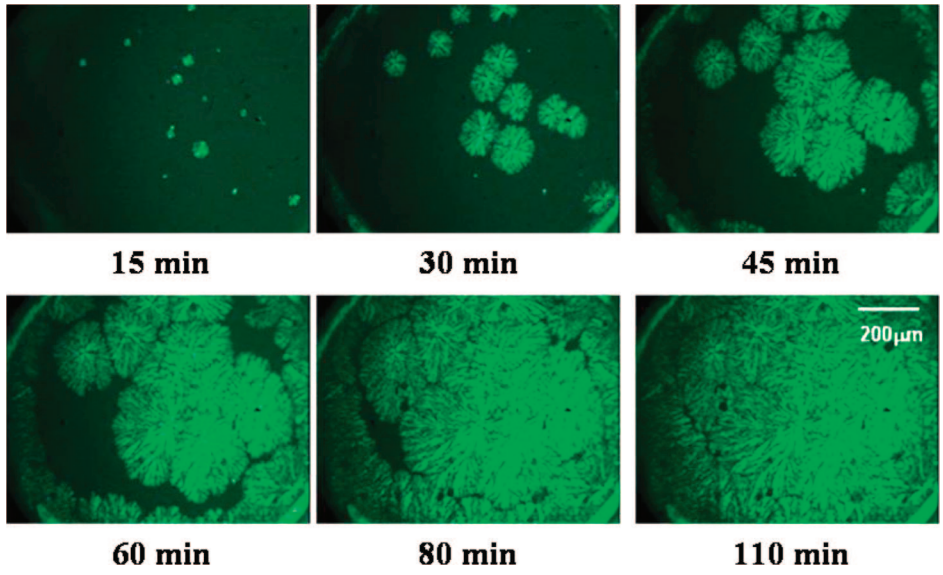

Figure 8. Time evolution of the PEO spherulites in the 30/70 PEO/DA blend undergoing photopolymerization induced crystallization at 48 °C, showing the spherulitic growth at near the core followed by the seaweed growth from the outer peripheral edge. The photoinitiator utilized was Rose Bengal at 1% of DA under green-filtered light illuminated at an intensity of 17 μW/cm^2.

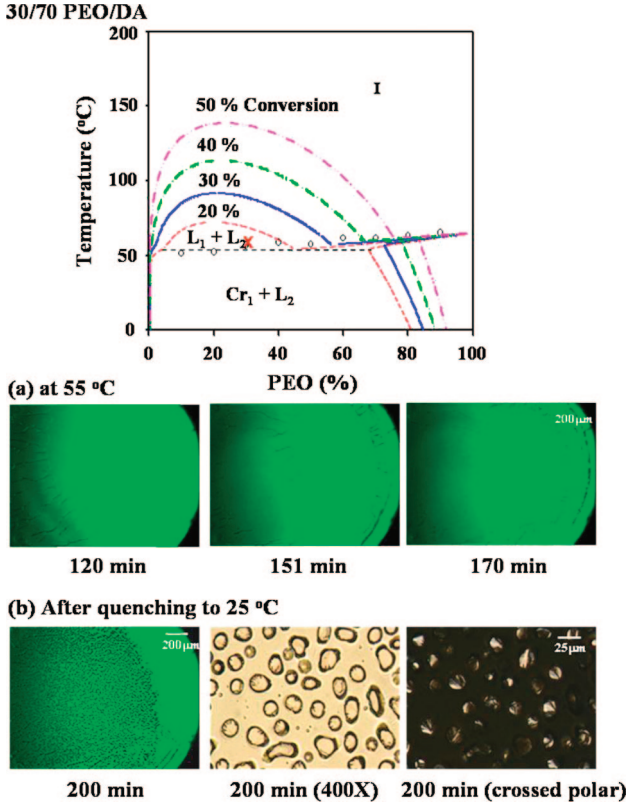

Figure 9. Occurrence of viscous fingering during photopolymerization of the 30/70 PEO/DA blend at 55 °C (i.e., above the crystal melting transition) showing the eventual break down to the liquid−liquid phase-separated domains. The photoinitiator utilized was Rose Bengal at 1% of DA under green-filtered light illuminated at an intensity of 17 μW/cm^2.

various exposure times. Figure 8 exhibits the emerged spherulites at the core, but the directional lamellar growth from the outer periphery (i.e., the circumference) of the illuminating beam toward the center for all concentrations investigated ranging from the 10/90 to 50/50 PEO/DA blends. This directional lamellar growth may be attributed to the photointensity gradient of the circular illuminating beam, i.e., with the intensity being strong in the middle, but it drop offs sharply at the circumference where crystal nucleation is initiated.

Another intriguing phenomenon is the viscous fingering when photopolymerization was carried out at elevated temperature of 55 °C, which is sufficiently higher than the melting temperatures of the original as well as that of the photocured 30/70 PEO/DA blends, and thus crystallization can no longer take place at such elevated temperatures. In the melt state, the viscous fingering starts at the circumference and propagates with elapsed reaction time toward the center by branching and tip splitting (Figure 9a). At 200 min, the fingers were broken down into smaller domains due to the instability of the viscous fluids. In the enlarged pictures, one can clearly identify the PEO-rich domains that show birefringent character upon quenching to room temperature (Figure 9b). The viscous fingering and concomitant liquid−liquid phase separation observed in the 30/70 PEO/DA blend can also be confirmed in the 40/60 (Figure 10a) and 50/50 PEO/DA (data not shown) compositions. This observation lends support to the idea of the competition between liquid−liquid phase separation and crystallization driven by photopolymerization. In this particular system, the PEO crystallization is dominant over the phase-separated domains, especially when the reaction temperature is 53 °C or lower. At 54 or 55 °C, the temperature is too high for the crystallization to occur, and thus only viscous fingering of PEO melt takes place within the DA continuum networks. This viscous fingering phenomenon may be a consequence of the mismatch of viscosities of the polymer melt and the network forming fluid, which may be attributed to the directional flow driven by the photointensity gradient during photopolymerization-induced liquid−liquid phase separation. At higher compositions such as 40/60 and 50/50, one can witness a similar temperature dependency on the crystal growth induced by photopolymerization (Figure 10b), i.e., exhibiting the directional growth in the Cr_1 + I gap epitaxially from the periphery of the illuminated beam and the viscous fingering in the L_1 + L_2 region.

Conclusions

We have demonstrated experimentally and theoretically that the PEO/DA blends are partially miscible with the solid−liquid phase diagram exhibiting the liquidus and solidus lines pertaining to the crystal−melt transition in conjunction with the binodal curves of the UCST phase diagram. The phase diagram of the

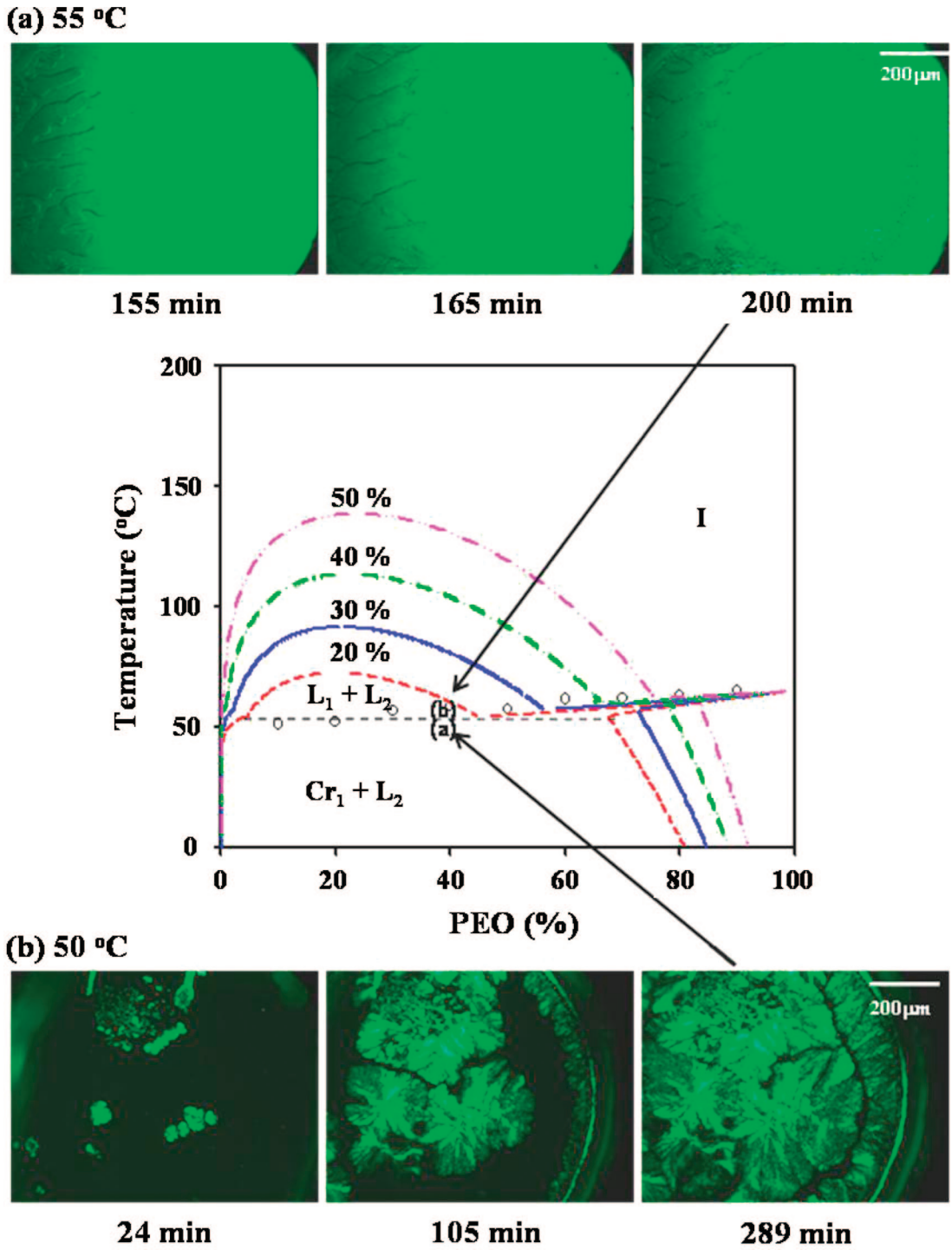

Figure 10. Emergence of (a) the viscous fingering pattern at a high temperature of 55 °C and (b) the hierarchical structures of PEO/DA 40/60 at 50 °C.

PEO/DA system consists of isotropic (I), the coexistence of crystal + liquid ($Cr_1 + L_2$), and the crystal + crystal ($Cr_1 + Cr_2$) regions. The Cr_1 gap corresponding to the PEO crystal is clearly discernible in the phase diagram, but the Cr_2 gap is extremely narrow as though it coincided virtually with the neat DA crystal axis. These self-consistently calculated coexistence regions have been further confirmed by means of time-resolved optical microscopy through inspection of the temporal evolution of the crystalline phase morphology following several temperature quenches into these individual regions. Various crystalline phase morphologies were observed including open to dense spherulitic morphologies coexisting with the isotropic matrix. At higher reaction temperatures above the T_m, viscous fingering (or fractal) growth takes place during photopolymerization, showing phase-separated domains within these emerging viscous fingering structures. However, these phase-separated domains tend to disappear if the reaction temperature were higher than the UCST, especially at low conversions.

Acknowledgment. Support of this work by the National Science Foundation through Grant DMR-0514942 is gratefully acknowledged.

References and Notes

(1) Tanaka, H.; Nishi, T. *Phys. Rev. Lett.* **1985**, *55*, 1102.
(2) Qiu, Z.; Ikehara, T.; Nishi, T. *Polymer* **2003**, *44*, 2799.
(3) Liu, A. S.; Liau, W. B.; Chiu, W. Y. *Macromolecules* **1998**, *31*, 6593.

(4) Drolet, F.; Elder, K. R.; Grant, M.; Kosterlitz, J. M. *Phys. Rev. E* **2000**, *61*, 6705.
(5) Kyu, T.; Chiu, H.-W.; Guenthner, A.; Okabe, Y.; Saito, H.; Inoue, T. *Phys. Rev. Lett.* **1999**, *83*, 2749.
(6) Xu, H.; Keawwattana, W.; Kyu, T. *J. Chem. Phys.* **2005**, *123*−8.
(7) Matkar, R. A.; Kyu, T. In *Polyolefin Blends*; Nwabunma, D., Kyu, T., Eds.; Wiley: New York, 2007; Chapter 16, p 473.
(8) Matkar, R. A.; Kyu, T. *J. Phys. Chem. B* **2006**, *110*, 12728.
(9) Matkar, R. A.; Kyu, T. *J. Phys. Chem. B* **2006**, *110*, 16059.
(10) Flory, P. J. *Principles of Polymer Chemistry*; Cornell University Press: Ithaca, NY, 1953.
(11) Chan, S.-K. *J. Chem. Phys.* **1977**, *67*, 5755.
(12) Harrowell, P. R.; Oxtoby, D. W. *J. Chem. Phys.* **1987**, *86*, 2932.
(13) Kobayashi, R. *Physica D* **1993**, *63*, 410.
(14) Kim, J. Y.; Cho, C. H.; Palffy-Muhoray, P.; Mustafa, M.; Kyu, T. *Phys. Rev. Lett.* **1993**, *71*, 2232.
(15) Inoue, T. *Prog. Polym. Sci.* **1995**, *20*, 119.
(16) Kyu, T.; Lee, J. H. *Phys. Rev. Lett.* **1996**, *76*, 3746.
(17) Kyu, T.; Chiu, H.-W. *Polymer* **2001**, *42*, 9173.
(18) Meng, S.; Kyu, T.; Natarajan, L. V.; Tondiglia, V. P.; Sutherland, R. L.; Bunning, T. J. *Macromolecules* **2005**, *38*, 4844.
(19) Park, S. J.; Rathi, P.; Kyu, T. *Phys. Rev. E* **2007**, *75*, 051804.
(20) Valdes-Aguilera, O.; Pathak, C. P.; Shi, J.; Watson, D.; Neckers, D. C. *Macromolecules* **1992**, *25*, 541.
(21) Bunning, T. J.; Natarajan, L. V.; Tondiglia, V. P.; Sutherland, R. L. *Annu. Rev. Mater. Sci.* **2000**, *30*, 83.
(22) Nishi, T.; Wang, T. T. *Macromolecules* **1975**, *8*, 909.
(23) Smith, P.; Manley, R. St. J. *Macromolecules* **1979**, *12*, 483.
(24) Wittmann, J. C.; Manley, R. St. J. *J. Polym. Sci., Polym. Phys. Ed.* **1977**, *15*, 1089.
(25) Daniel, C.; Menelle, A.; Brulet, A.; Guenet, J. M. *Polymer* **1997**, *38*, 4193.
(26) Ray, B.; Elhasri, S.; Thierry, A.; Marie, P.; Guenet, J. M. *Macromolecules* **2002**, *35*, 9730.
(27) Malik, S.; Rochas, C.; Guenet, J. M. *Macromolecules* **2005**, *38*, 4888.
(28) Kerridge, R. *J. Am. Chem. Soc.* **1952**, *1952*, 4577.
(29) Duran, H.; Meng, S.; Kim, N.; Hu, J.; Kyu, T.; Natarajan, L. V.; Tondiglia, V. P.; Bunning, T. J. *Polymer* **2008**, *49*, 534.

MA802161C